Precision and reliability of periodically and quasiperiodically driven integrate-and-fire neurons

P. H. E. Tiesinga
Sloan-Swartz Center for Theoretical Neurobiology and Computational Neurobiology Laboratory, Salk Institute, 10010 North Torrey Pines Road, La Jolla, California 92037
(Received 17 October 2001; published 2 April 2002)

Neurons in the brain communicate via trains of all-or-none electric events known as spikes. How the brain encodes information using spikes—the neural code—remains elusive. Here the robustness against noise of stimulus-induced neural spike trains is studied in terms of attractors and bifurcations. The dynamics of model neurons converges after a transient onto an attractor yielding a reproducible sequence of spike times. At a bifurcation point the spike times on the attractor change discontinuously when a parameter is varied. Reliability, the stability of the attractor against noise, is reduced when the neuron operates close to a bifurcation point. We determined using analytical spike-time maps the attractor and bifurcation structure of an integrate-and-fire model neuron driven by a periodic or a quasiperiodic piecewise constant current and investigated the stability of attractors against noise. The integrate-and-fire model neuron became mode locked to the periodic current with a rational winding number p/q and produced p spikes per q cycles. There were q attractors. $p{:}q$ mode-locking regions formed Arnold tongues. In the model, reliability was the highest during 1:1 mode locking when there was only one attractor, as was also observed in recent experiments. The quasiperiodically driven neuron mode locked to either one of the two drive periods, or to a linear combination of both of them. Mode-locking regions were organized in Arnold tongues and reliability was again highest when there was only one attractor. These results show that neuronal reliability in response to the rhythmic drive generated by synchronized networks of neurons is profoundly influenced by the location of the Arnold tongues in parameter space.

DOI: 10.1103/PhysRevE.65.041913 PACS number(s): 87.19.La, 87.19.Dd, 87.17.Aa

I. INTRODUCTION

Although spike trains in the cerebral cortex are highly variable (for a review see [1]), neurons can fire with high temporal precision and reliability *in vitro* [2–8]. Precision is defined here as the inverse of the temporal jitter in the spike time and reliability as the reproducibility of spikes across different presentations of the same stimulus (trials). Information-theoretical analyses of the neuronal spike trains in the lateral geniculate nucleus indicate that precise spike times contain more information about the stimulus than firing rate alone [9,10]. It is unknown how these precise spike times are used in the cortex [1,11–15].

If a feature is present in the spike-train response to one stimulus across multiple trials it can form the basis of a neuronal code. Spike-time reliability is a measure for the reproducibility of individual spike times across trials [16]. Neurons produce a reliable sequence of spike times in response to some inputs and respond unreliably to others. In the *in vitro* slice, neurons fire reliably when injected with a random current containing high frequency components, but they fire unreliably when driven with a low pass or constant current [16–22]. Sinusoidally driven neurons show resonances in the reliability as a function of drive frequency [23–25].

Recently, we proposed a framework for understanding the reliability of neuronal discharge in terms of two mathematical concepts, attractor and bifurcation [26]. We briefly review these previous results to set the stage for the issues addressed in this paper. Examples of attractors of an integrate-and-fire (IAF) model neuron are shown in Fig. 1. The model neuron was driven by a quasiperiodic current consisting of the sum of two sinusoids with an irrational ratio between their frequencies. There were two attractors. From one set of initial voltages, the voltage converged to the first attractor [Fig. 1(Aa)] and from a different set it converged to the second attractor [Fig. 1(Ab)]. Each attractor corresponded to a distinct sequence of spike times [Fig. 1(Ac)]. In the presence of weak noise the neuron also converged to the attractor, but the voltage fluctuated around the zero noise value. When the neuron remained on the attractor it produced the same sequence of spike times on each trial and the spike-time variance across trials was proportional to the noise variance [26]. The driving stimulus can be parametrized in terms of, for instance, the amplitude, the frequency, and the mean. A bifurcation point is a stimulus parameter value at which the attractor voltage and output spike train change discontinuously when the parameter is varied by a small amount. Noise sensitivity of the attractor (hence reliability) was connected to the presence of bifurcations. For parameters close to a bifurcation point, noise can induce a deviation from the attractor so that different spike trains are obtained across different trials, reducing reliability. Two possible deviations are shown in Fig. 1(Bb). Two spike trains were considered different when at least one spike time in the first spike train differed by more than the typical jitter from all the spike times in the second spike train [27] (see also Sec. V C). The above framework makes it possible to assess the reliability for many different noise strengths by varying stimulus parameters and determining bifurcation points.

The reliability of the neuronal spike-train response to a random fluctuating current is different compared with the reliability in response to a periodic driving current. These differences are related to the bifurcation structure: mode locking to periodic drives leads to Arnold tongues that are absent for a random fluctuating drive. A quasiperiodic drive is not periodic but nonetheless has long time correlations. It is intermediate between a periodic and random fluctuating drive. Here we compare the bifurcation structure of an

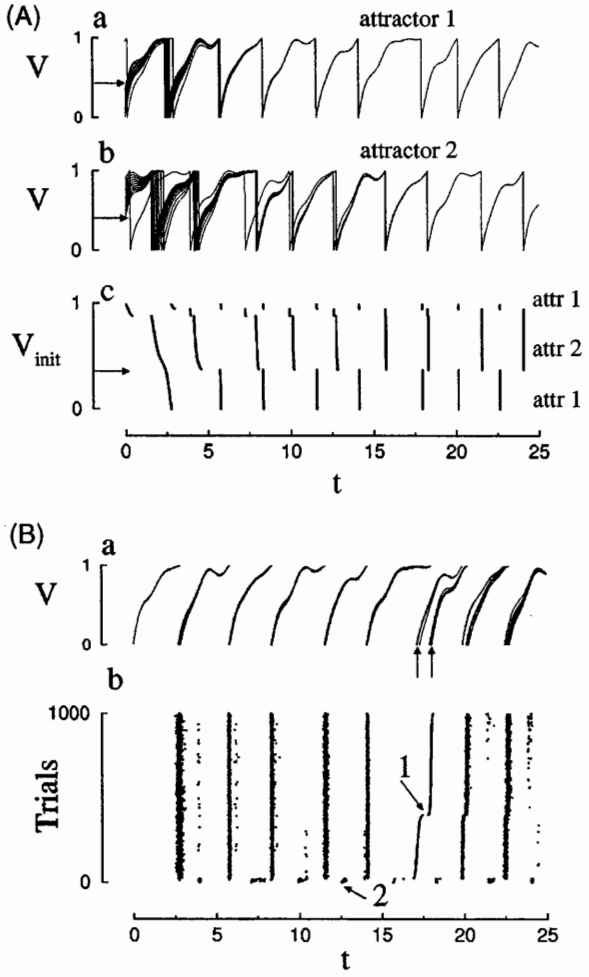

FIG. 1. Attractors of neurons driven by a quasiperiodic current. (A) The voltage was plotted as a function of time starting from different initial voltage values V_{init}. When the voltage reaches 1, a spike is emitted and the voltage is reset to 0. The dynamics converged to either of two different attractors, (a) and (b), respectively. The attractors remained distinct for long times. However, we did not establish whether this holds for arbitrarily long times. (c) The corresponding spike times (x ordinate) as a function of V_{init} (y ordinate). The two attractors are labeled in the graph by attr1 and attr2, respectively. Arrows indicate one of the two boundaries between the basins of attraction. (B) Dynamics in the presence of noise. (a) 10 voltage traces and (b) 1000 spike trains (trials) each starting at $V_{init}=0$ but with a different realization of the noise. The neuron could remain on one attractor, or (1) deviate from it during a few spike times, or (2) make a transition to the other attractor. Spike trains were ordered on the value of the first spike time after $t=15$. Arrows in (a) indicate the voltage curves corresponding to the two possible spike times in (b,1).

integrate-and-fire model neuron driven by a periodic piecewise constant current with that of a neuron driven by a quasiperiodic piecewise constant current. The numerical calculation was speeded up significantly since it was possible to derive an analytical spike-time map representing the dynamics of neurons driven by piecewise constant currents. We find for both periodic and quasiperiodic drives that (1) mode-locking regions are organized in Arnold tongues and (2) reliability is highest when there is only one attractor.

II. METHODS

A. Simulation algorithm

The membrane potential V of an integrate-and-fire model neuron driven by a fluctuating current satisfied [28],

$$\frac{dV}{dt}=-V+I+f(t)+\xi(t), \tag{1}$$

where I was a time-independent driving current, $f(t)$ was a fluctuating current, and ξ was a white noise current, with zero mean and variance D, that represented the effects of intrinsic noise. When the voltage V reached threshold, $V(t^-)=1$, a spike was emitted and the voltage was reset to zero, $V(t^+)=0$. Here t^- was the limit to t from below, and t^+ was the limit to t from above. The first term on the right hand side of Eq. (1) represented the decay of the voltage to the resting membrane potential, $V=0$. Dimensionless units were used, one voltage unit corresponded to the distance between the resting membrane potential and action potential threshold, ≈ 20 mV [28]; one time unit corresponded to the membrane time constant, approximately equal to 10–40 ms [28]. With the membrane capacitance taken equal to 1 μF/cm^2, a driving current equal to 1 corresponds to 0.5–2 μA/cm^2.

A periodic or quasiperiodic piecewise constant current $f(t)$ was injected into the neuron. The periodic current was equal to $f(t)=-A$ when $0\leq \mathrm{mod}(t,T)<T/2$ and $f(t)=A$ otherwise. Here A was the amplitude of the drive, T was the period, and the frequency was $\omega=2\pi/T$. The quasiperiodic current consisted of the sum of two periodic currents, with periods T_1 and T_2 and a relative phase $\Delta\phi$, $f(t)=A_1I_1(t+\Delta\phi)+A_2I_2(t)$. Here A_1 and A_2 were the drive amplitudes and $\omega_1=2\pi/T_1$, $\omega_2=2\pi/T_2$ were the drive frequencies. $I_1(t)=-1$ when $0\leq \mathrm{mod}(t,T_1)<T_1/2$ and 1, otherwise. $I_2(t)=-1$ when $0\leq \mathrm{mod}(t,T_2)<T_2/2$ and 1, otherwise. In the simulations presented here $\Delta\phi=0$.

The voltage of the integrate-and-fire model neuron was integrated analytically [Eq. (1)]. When the last spike occurred at t_1, $V(t_1^+)=0$, the voltage at a later time, but before the next spike, was

$$V(t|t_1)=I(1-e^{-(t-t_1)})+e^{-t}\int_{t_1}^{t} ds\, e^s[f(s)+\xi(s)]. \tag{2}$$

The next spike time t_2 was the smallest solution of the equation $V(t_2|t_1)=1$.

The equation for periodic and quasiperiodic piecewise constant driving current was analytically inverted to yield a spike-time map M. The map determined the next spike time t_{n+1} as a function of the previous spike time t_n, $t_{n+1}=M(t_n)$. Details of the calculation are given in the Appendix. Simulations based on iteration of the spike-time map were up to two orders of magnitude faster than direct integration and yielded spike times that were accurate to machine precision for zero noise and accurate to the square root of machine precision for simulations with noise. The accuracy of the spike-time map for zero noise was checked against results from direct integration using fourth-order

Runge-Kutta [29]. Threshold crossings (the spike times) were determined by linear interpolation. Note that for linearly interpolated spike times a second-order Runge-Kutta would also have been adequate [30].

B. Spike-time statistics

The map $t_{n+1}=M(t_n)$ was iterated starting from the initial spike time $t_0=t_{init}$ to obtain 2000–10 000 spike times. In most cases we took $t_{init}=0$. The first 20% of the spike times were discarded as a transient, the remaining $N_s=1600$–8000 were used for further analysis as described below. The periodically driven noiseless integrate-and-fire neuron converged after a transient onto a periodic attractor. The mean interspike interval (ISI) was,

$$\tau=\frac{1}{N_s-1}\sum_{n=1}^{N_s-1}\tau_n, \tag{3}$$

where N_s was the number of spikes in the simulation run, and $\tau_n=t_{n+1}-t_n$. The winding number, defined as the average number of spikes per cycle, $\langle N\rangle=T/\tau$, was approximately equal to a fraction p/q, here T was the period.

The neuron emitted p spikes in q cycles, and the spike train repeated itself after q cycles. The spike phase of spike time t_n was $\psi_n=\mathrm{mod}(t_n,T)/T$. On the attractor the ψ_n time series was periodic with period p, $\psi_{m+p}=\psi_{m+2p}=\cdots=\Psi_m$. Hence the neuron spiked only at p different phases,

$$\Psi_m=\frac{p}{N_s}\sum_{n=0}^{N_s/p-1}\psi_{m+np}, \tag{4}$$

for $m=1,\ldots,p$. In the presence of noise there was spike-phase jitter, the standard deviation of the spike phase was

$$\sigma^{(p)}=\sqrt{\frac{1}{p}\sum_{m=1}^{p}(\sigma_m^{(p)})^2},$$

$$(\sigma_m^{(p)})^2=\frac{p}{N_s}\sum_{n=0}^{N_s/p-1}\psi_{m+np}^2-\Psi_m^2. \tag{5}$$

In Eqs. (4) and (5) it was assumed that the number of spikes N_s is a multiple of p, during the calculation the appropriate changes were made when this was not the case. Note that p needed to be estimated from $\langle N\rangle$ prior to calculating $\sigma^{(p)}$.

For a quasiperiodic drive, there were two periods. The spike phase with respect to T_1 was $\psi_n^1=\mathrm{mod}(t_n,T_1)/T_1$ and with respect to T_2 it was $\psi_n^2=\mathrm{mod}(t_n,T_2)/T_2$. The mean and variance of the phase were defined in analogy to Eqs. (4) and (5).

C. Arnold tongues

Regions in parameter space with the same winding number $\langle N\rangle=p/q$ formed Arnold tongues. The Arnold-tongue structure was determined for a number of parameter combinations, specifically, (ω,A), (A_2,I), and (ω,D). A two-dimensional grid (x_i,y_j) was constructed, here $i=1,\ldots,N_x$; $j=1,\ldots,N_y$; and x and y were ω, A, A_2, I, or D. The grid was specified by the starting point x_{min}, end point x_{max}, and the number of grid points N_x. The same notation holds for y and is not repeated here and in what follows. We either used a linear grid,

$$x_i=x_{min}+\frac{i-1}{N_x-1}(x_{max}-x_{min}),$$

$i=1,\ldots,N_x$, or a logarithmic grid,

$$x_i=\exp\left[l_{x,min}+\frac{i-1}{N_x-1}(l_{x,max}-l_{x,min})\right],$$

here $i=1,\ldots,N_x$, $l_{x,min}=\ln x_{min}$, and $l_{x,max}=\ln x_{max}$.

The Arnold-tongue structure was determined based on the winding number calculated from 1600–8000 spike times. Grid points (ω_i,A_j) or $(A_{2,i},I_j)$ with a winding number satisfying $|\langle N\rangle-p/q|<1/400$ were considered part of the p:q Arnold tongue. Alternatively, for zero noise, Arnold Tongues could also be determined by simultaneously solving a large set of algebraic equations as in Ref. [31]. Here we use a brute force approach made feasible by the computationally efficient implementation of the spike-time map.

A different procedure was used for the construction in the (ω,D) plane. D_j was taken on a logarithmic grid. The p:q values for a given ω were determined for $D=0$. These p values were then used to calculate $\sigma^{(p)}$ as a function of D for nonzero D. For small D values, $\sigma^{(p)}\propto\sqrt{D}$ [32]. The first $N_f=7-10$ nonzero D_j values in the simulation run were used to fit $\eta_j=\ln\sigma^{(p)}(D_j)$ to $\ln\alpha_1+\alpha_2\ln D_j$, here α_1 and α_2 were fitting parameters. The fit was accepted when

$$\frac{1}{N_f}\sum_{j=1}^{N_f}(\eta_j-\ln\alpha_1-\alpha_2\ln D_j)^2<0.1,$$

and $0.45<\alpha_2<0.55$. A grid point (ω_i,D_j), with $j>N_f$, was part of the p:q Arnold tongue when

$$\frac{\sigma^{(p)}(D_j)-\alpha_1 D_j^{\alpha_2}}{\sigma^{(p)}(D_j)}<0.10.$$

Determining the Arnold-tongue structure is equivalent to finding the bifurcations for which the winding number changes discontinuously. A method for determining bifurcations in the presence of noise was recently presented in Refs. [33,34]. It involved constructing the phase transition matrix—the probability distribution of the phase of the next spike time conditional on the phase of the previous spike time—and performing a spectral analysis on it.

III. MODE LOCKING TO PERIODIC DRIVES

The dynamical equations for the IAF model neuron were analytically integrated to produce a spike-time map that predicted the next spike time given the previous spike time. The derivation and numerical implementation of the map is described in Sec. II; further details are in the Appendix. The map was iterated starting from an initial spike time $t_{init}=0$. The amplitude A was 0.4 and the drive frequency $\omega/2\pi$

$=1/T$ was varied, here T was the drive period (cycle length). For a given frequency ω the neuron converged, after a brief transient, on to a periodic attractor and was then mode locked to the drive. The resulting spike train was periodic with a period equal to q drive cycles, during which p spikes were emitted. The average interspike interval was qT/p. The winding number $\langle N\rangle$ is the average number of spikes per drive cycle; during mode locking it was rational and equal to p/q, where p and q were positive integers.

For a constant driving current $I=1.5$ and $A=0$, the average interspike interval was approximately 1.1. For a finite amplitude, $A=0.4$, the neuron was 1:1 mode locked when the period was close to 1.1. This led to a step of constant winding number, $p/q=1$, in the $\langle N\rangle$ versus ω characteristic [Fig. 2(Aa)]. There were also steps for other rational winding numbers and the $\langle N\rangle$-ω graph had the appearance of a staircase. The steps with low q values were wide, with the 1:1 step being the widest.

During p:q mode locking the neuron fired at p different phases Ψ_m, $m=1,\ldots,p$. Here the phase was defined as the spike-time modulo the period, divided by the period (see, Sec. II). On a mode-locking step the winding number was constant, whereas the spike phase increased with ω. For instance, during 1:1 entrainment Ψ_1 was equal to $\frac{1}{2}$ on the left hand side of the step and increased to 1 on the right hand side of the step [Fig. 2(Ab)].

There were q different attractors of the dynamics for p:q mode locking. The other attractors were obtained from a given attractor by shifting over multiples of the drive cycle. This procedure is illustrated in Fig. 2(B) for $N=\frac{2}{3}$. On the first attractor, the neuron fired at phase Ψ_1 on the first cycle, at phase Ψ_2 on the second cycle, and did not fire on the third cycle. This spike pattern then repeated itself. A second attractor was obtained by shifting this pattern over one period, the neuron then did not fire during the first cycle, fired at Ψ_1 on the second and at Ψ_2 on the third cycle. A third attractor was obtained by shifting the first one over two drive cycles. This multistability of the spike times should not be confused with a multistability that occurs for a noninvertible circle map (see, for instance, Ref. [35]). In that case there are two or more stable solutions with *different* winding numbers and the Arnold tongues intersect.

From a given initial condition only one attractor was obtained. The set of initial conditions from which a given attractor was obtained is the basin of attraction. In the spike-time map formulation of the dynamics the initial condition was the first spike time. All q attractors were reached when the first spike time was varied between 0 and qT [Fig. 2(C)]. When the dynamics were integrated in time using Eq. (1), the initial condition was the voltage V_{init} at the start of the simulation. All attractors were reached when V_{init} was varied between 0 and 1 (results not shown, see also [26]).

The number of attractors q varied nonmonotonically as a function of ω. For instance, between the 2:1 and 1:1 steps, all other q values were obtained [for clarity only data for $q\leq 4$ were shown in Fig. 2(Ac)]. The spike times (and phases) changed discontinuously during a transition from one q value to another. Hence, when q changed a spike-time bifurcation

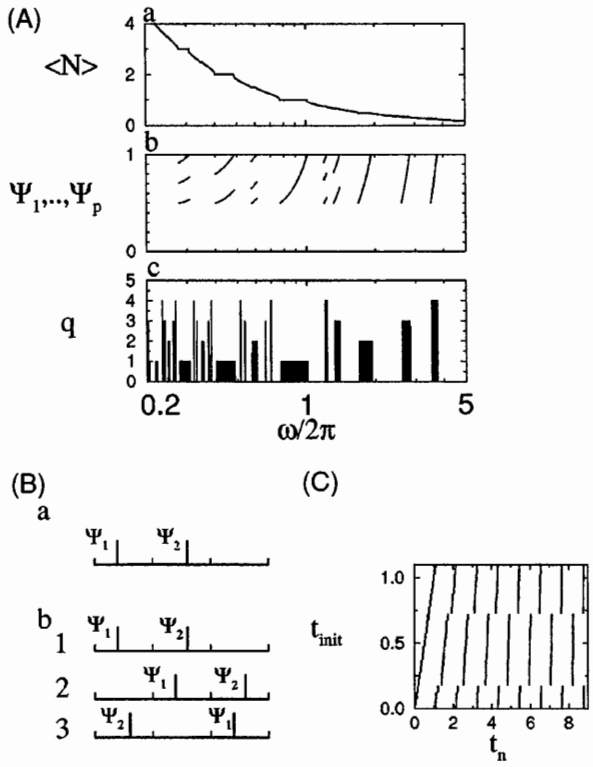

FIG. 2. (A) The integrate-and-fire neuron was mode locked to a periodic piecewise constant current. (a) The average number of spikes per cycle, $\langle N\rangle=T/\tau$, vs frequency $\omega=2\pi/T$. On the mode-locking steps $\langle N\rangle$ was constant and equal to a fraction p/q, the neuron then emitted p spikes in q cycles at phases $\Psi_1,\ldots,\Psi_p$. (b) The phases for steps with $p\leq 3$ and (c) the number of attractors, q, with $q\leq 4$, were plotted vs ω. Averages were over 3200 spikes after discarding the first 800 spikes. (B) The number of attractors was equal to q. (a) The winding number was $\langle N\rangle=\frac{2}{3}$, the neuron emitted 2 spikes in 3 cycles with phases Ψ_1 and Ψ_2. The spike train was periodic with period of 3 cycles. The distance between two small ticks is the cycle length T. (b) Two other attractors were obtained by shifting (1) the first attractor over (2) one and (3) two periods T, respectively. (C) Neuron that was 1:2 mode locked to a drive with $T=0.56$. All q attractors were reached from initial spike times t_{init} in the interval between 0 and qT. Each tick represented a spike, its x ordinate was the spike time t_n and its y ordinate was given by the starting spike time of the trial. (A)–(C) Parameters were $I=1.5$, $A=0.4$, and $D=0$.

occurred, and the frequency value at which this happened was a bifurcation point. The bifurcation points were not distributed uniformly across the frequency axis: there were no bifurcation points between $\omega/2\pi\approx 0.75$ and $\omega/2\pi\approx 1.0$, and many between $\omega/2\pi\approx 0.5$ and $\omega/2\pi\approx 0.75$.

Reliability was defined as the stability of the attractor against intrinsic noise [27]. The discharge was unreliable when noise induced transitions from one attractor to a different attractor, or when it induced an extra spike or prevented a spike from occurring when there was only one stable attractor. The attractors were not equally stable for all parameter values corresponding to the same winding number. Two frequency values for which 1:1 entrainment was obtained were considered as an example, $\omega/2\pi=0.7752$ with Ψ_1

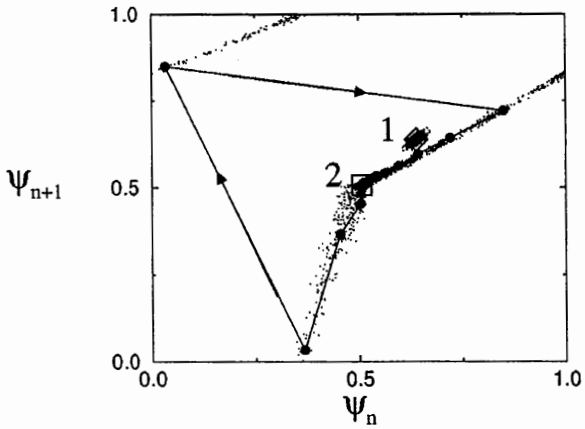

FIG. 3. Spike-phase return map during 1:1 mode locking in the presence of noise. In the return map the next phase ψ_{n+1} was plotted vs the previous phase ψ_n. In the absence of noise, the return map consisted of a single point with coordinates (Ψ_1,Ψ_1), here Ψ_1 was the spike phase on the attractor. Two points were shown, (1, open diamond) drive period $T=1.15$ ($\omega/2\pi=0.8696$) in the middle of the step and (2, open square) $T=1.29$ ($\omega/2\pi=0.7752$) close to the edge of the step. In the presence of noise, $D=10^{-4}$, the attractor for $T=1.15$ was stable. The return map consisted of a cloud of points around the zero-noise return map (1). For $T=1.29$, the attractor was unstable against noise. Most points were close to the zero-noise return map (2). However, sometimes an extra spike was introduced with a phase $\psi_n<0.5$, the neuron then deviated from the attractor and the corresponding points formed an open orbit. One such orbit was shown as large filled circles connected by arrows that indicated the direction in which the orbit was traversed. 3000 iterates were used to construct the return map, the first 500 iterates were discarded. Other parameters were $I=1.5$ and $A=0.4$.

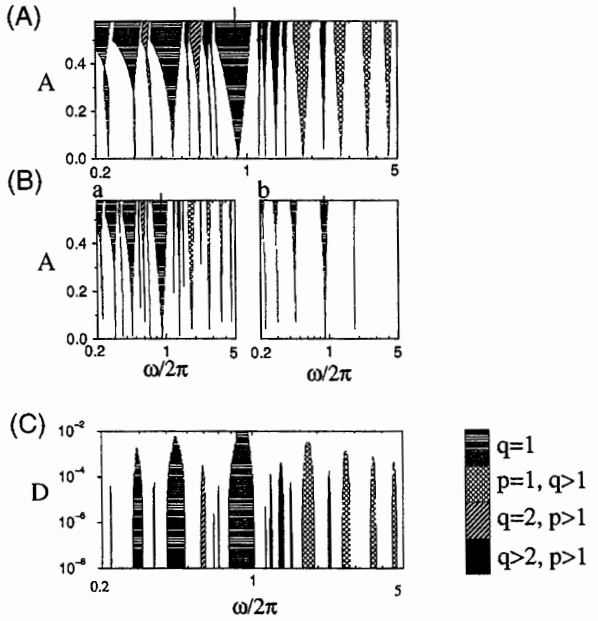

FIG. 4. Arnold tongues for a neuron driven by a piecewise constant periodic current. Arnold tongues were constructed as described in Sec. II, the set of points with the same winding number $\langle N\rangle=p/q$ was coded for its $p:q$ value as shown in the legend to the right of (C). For clarity only a few of the Arnold tongues are shown in the graph. (A) $N_\omega=5000$, $N_A=59$, $D=0$; (B) $N_\omega=1000$ and $N_A=17$, with noise strength D equal to (a) 1×10^{-4} and (b) 4×10^{-3}. (C) The grid along the D axis consisted of $N_D=50$ values between $D=1\times10^{-8}$ and $D=1\times10^{-2}$, N_ω was 1000 and $A=0.4$. Averages were over 3200 spikes after discarding a transient of 800 spikes. The driving current was $I=1.5$. Arrows in (A),(B) indicate the 1:1 mode-locking Arnold tongues.

$=0.5067$ near the left hand side of the step and $\omega/2\pi=0.8696$ with $\Psi_1=0.6383$ in the middle of the step. The return map, where the next phase ψ_{n+1} was plotted vs the previous phase ψ_n, was a single point (Ψ_1,Ψ_1) in the absence of noise (Fig. 3). This point was the fixed point of the map. For nonzero noise, $D=10^{-4}$, and $\omega/2\pi=0.8696$, the return map consisted of a cloud of points distributed around the zero-noise point (Ψ_1,Ψ_1). The phase fluctuated around the average value and the attractor was stable against noise. However, for $\omega/2\pi=0.7752$, the phase took any value between 0 and 1. Noise induced an extra spike on some cycles at a phase that was far from the fixed point of the dynamics, this resulted in large deviations of the spike phase. It took a number of cycles for the neuron to return to the attractor. Hence, the attractor was unstable against noise for the given noise strength. Note that in the deterministic case the stability of the solution is given by the Lyapunov exponent. For all the frequency values on the step the Lyapunov exponent was negative and the solution was stable [31,35]. In general, the closer the neuron was to the edge of a step—a bifurcation point—the less stable the attractor was to intrinsic noise. We observed that attractors for mode-locking at higher q values were less stable when the step width was smaller. For the piecewise constant periodic current considered in Fig. 2, the fixed point phases only took values between $\frac{1}{2}$ and 1. The unstable edges of the step corresponded to the values $\frac{1}{2}$ and 1. For $p>1$, multiple phases have to fit in this interval. Hence, for higher p there was at least one phase Ψ_m, $(m=1,\ldots,p)$ close to the edge—the resulting attractor was less stable against noise.

Next the amplitude A was varied. For $A=0$, when there was no periodic drive, the neuron was "mode locked" at discrete frequencies values $\omega/2\pi=p/q\tau$, where $\tau\approx1.1$ is the average interspike interval of the neuron [Eq. (3) in Sec. II]. When A was nonzero, $p:q$ mode locking occurred in a range of frequency values around these discrete points. The regions in the ω–A parameter space where the neuron was $p:q$ mode locked formed Arnold tongues [Fig. 4(A)] [31]. The width of the $p:q$ step—the frequency range for which mode locking was obtained—generally increased with A. However, for low frequencies, $\omega/2\pi<1$ and $A<0.4$ the width (and also the neuron's firing rate) varied nonmonotonically with amplitude. This was further investigated by comparing the dynamics on the 3:1 step for $A=0.3$ and $A=0.4$. For $A=0.4$, the 3 spike phases on the 3:1 step were between $\frac{1}{2}$ and 1 [Fig. 2(Ab)], and from almost any initial condition the neuron converged exponentially fast to the attractor [Fig. 5(Bb)]. In contrast, for $A=0.3$, the spike phases took values between 0 and 1 [Fig. 5(Ab)], and convergence was slow when the simulation was started at a spike phase far from the attractor [Fig. 5(Ba)].

The Arnold-tongue structure in the presence of noise was

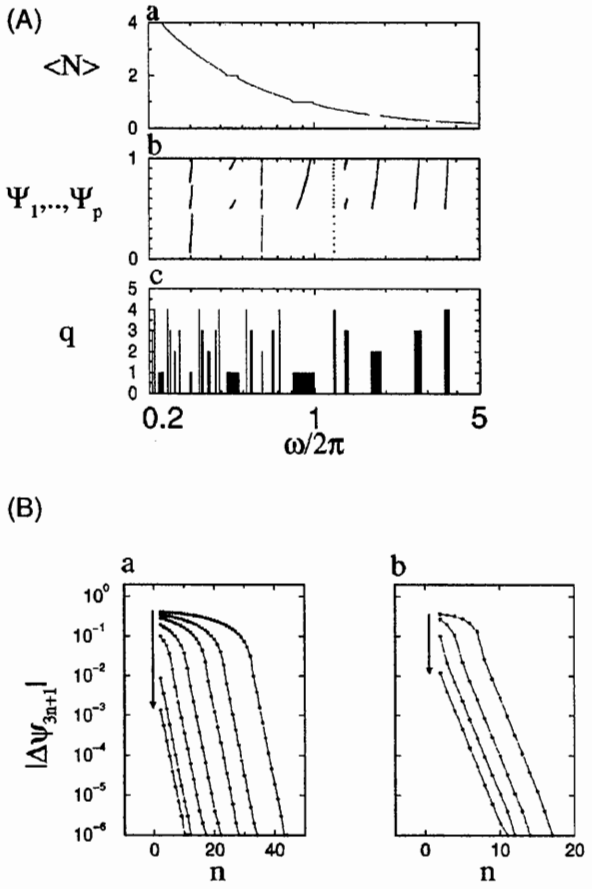

FIG. 5. (A) Mode-locking steps for $A=0.3$. (a) The winding number $\langle N\rangle$, (b) the spike phases, $\Psi_1,\ldots,\Psi_p$, and (c) the number of attractors q as a function of frequency ω. For clarity only data for $p\leq 3$ and $q\leq 4$ are shown in b and c, respectively. Note that in (b) the spike phases for small $\omega/2\pi$ took values between 0 and 1. Averages were over 3200 spike times after discarding a transient of 800. (B) Convergence to the attractor during 3:1 mode locking was slower for (a) $A=0.3$ compared with (b) $A=0.4$. The spike phases on the attractor were Ψ_1, Ψ_2, and Ψ_3. The distance to the first one, $\Delta\psi_{3n+1}=\psi_{3n+1}-\Psi_1$, was plotted as a function of n starting from different initial spike times t_{init} from the basin of attraction of one of the three attractors. Here ψ_{3n+1} was the spike phase of the $(3n+1)$th spike time t_{3n+1}. From top to bottom (in the direction of the arrow), t_{init} was (a) 0.3, 0.7, 1.0, 1.3, 1.6, and 1.7; (b) 0.5, 0.7, 1.1, and 1.7. The last part of the trajectories was linear on a log scale and corresponded to exponential convergence onto the attractor. Other parameters were $I=1.5$, $D=0$, and in (B) $T=3.32$.

studied [Fig. 4(B)]. When the neuron remained on the attractor there was jitter in the spike times, but each spike that was present in the zero-noise spike train did occur. Hence, the average number of spikes per cycle, $\langle N\rangle$, was unchanged and equal to p/q. When the value of $\langle N\rangle$ obtained in the simulations was within $\frac{1}{400}$ of p/q it was considered part of the p:q Arnold tongue. For weak noise, $D=10^{-4}$, the Arnold-tongue structure was virtually identical to the $D=0$ structure [Fig. 4(Ba)]. Only points near the edge of the tongue were unstable, as noise induced transitions between attractors or led to missing or extra spikes. Note that these extra or missing spikes did not cancel out in the temporal average: Near the left hand side edge there could only be extra spikes, increasing $\langle N\rangle$, whereas near the right hand side there could only be missing spikes, reducing $\langle N\rangle$. Arnold tongues with high p or q values were also unstable, however, these were not resolved on the parameter grid and their absence could not be observed in the figure. For higher noise levels, $D=4\times10^{-3}$, only the $q=1$ steps remained and their width was much reduced compared with $D=0$ [Fig. 4(Bb)].

The mode-locking regions were also determined as a function of noise strength for a fixed amplitude $A=0.4$ [Fig. 4(C)]. The method for their construction was given in Sec. II. Briefly, the winding number for $D=0$ was determined numerically yielding a value for p and q. That p value was used to calculate $\sigma^{(p)}$ [Eq. (5)]. When $\sigma^{(p)}$ was proportional to $\sqrt{D}$ the grid point was considered part of the p:q Arnold tongue. The width of the tongue (step width) decreased as a function of D, since more and more points close to the edge became unstable. 1:1 mode locking was most stable; for $D=10^{-2}$, the 1:1 step was still present, whereas other steps had become unstable or could not be resolved on the parameter grid used for the simulations.

IV. MODE-LOCKING TO A QUASIPERIODIC CURRENT

The behavior of neurons driven by a quasiperiodic current was examined using the analytical spike-time map derived for a piecewise constant current drive. The quasiperiodic drive is intermediate between a periodic and a random (uncorrelated) drive. For a periodic drive, mode-locking regions are organized in Arnold tongues, unlike the mode-locking regions for a random drive. Hence, the question is whether mode-locking regions for a quasiperiodic drive are organized in Arnold tongues and how the reliability is related to the winding number(s).

The driving current was the sum of two periodic piecewise constant currents with periods T_1, T_2 and amplitudes A_1 and A_2, respectively. Here we used $T_1=2$ and $T_2=2\sqrt{2}$. In order to keep T_1/T_2 irrational we varied the driving current I instead of either T_1 or T_2 as was the case in the preceding section.

For a drive only containing the T_1 component, steps in the number of spikes per cycle, $\langle N_1\rangle=T_1/\tau$, as a function of I were obtained [Fig. 6(Aa)]. Here τ was the mean interspike interval. The steps were at rational values $\langle N\rangle=p_1/q_1$, hence the neuron produced p_1 spikes at phases $\Psi_1,\ldots,\Psi_{p_1}$ in q_1 cycles. The spike train was periodic with period q_1T_1. The phase of spike time t was defined as $\psi^1=\mathrm{mod}(t,T_1)/T_1$. The same was true when only the T_2 component was present [Fig. 6(Ab)], in that case the winding number was $\langle N_2\rangle=T_2/\tau=p_2/q_2$ and the phase was defined as $\psi^2=\mathrm{mod}(t,T_2)/T_2$.

When both components were present, there were steps with either a rational winding number with respect to T_1, $\langle N_1\rangle=p_1/q_1$ [Fig. 6(Aa)] or with respect to T_2, $\langle N_2\rangle=p_2/q_2$ [Fig. 6(Ab)].

The parameter regions in (I,A_2) space with a fixed value of p_1/q_1 or p_2/q_2 were organized in Arnold tongues [Fig. 6(Ac)]. For $A_2=0$, only the T_1 mode locking was obtained.

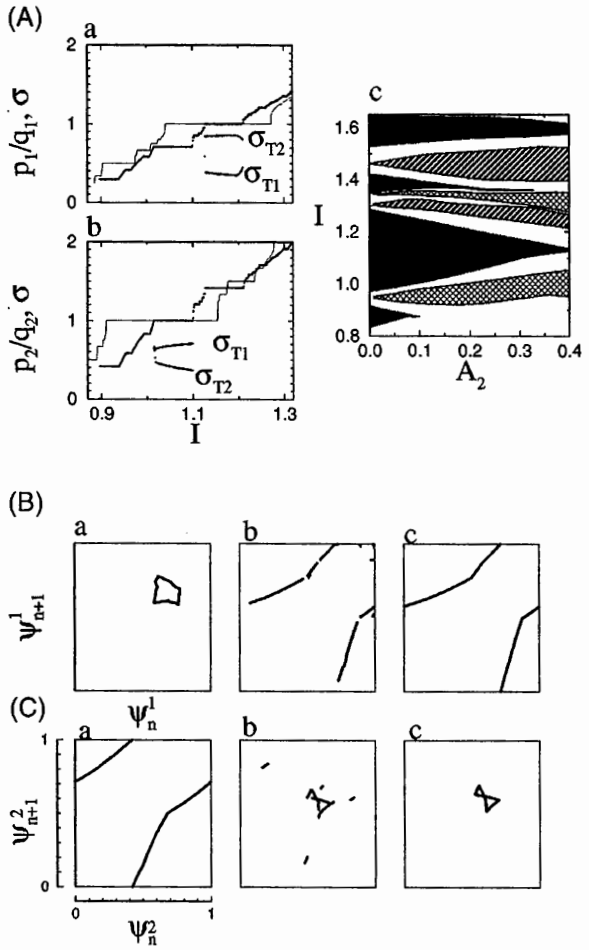

FIG. 6. Mode locking to a quasiperiodic drive yielded Arnold tongues. (A) There were two sets of winding numbers, (a) $\langle N\rangle = T_1/\tau$ equal to p_1/q_1 for T_1 mode locking and (b) T_2/τ equal to p_2/q_2 for T_2 mode locking, here τ was the average interspike interval. Three sets of parameters were considered, $A_1=0.25$, $A_2=0$ (a, continuous line); $A_1=0$, $A_2=0.25$ (b, continuous line); $A_1=0.125$, $A_2=0.125$ (a,b, small circles). The standard deviation σ_{T1} and σ_{T2} of the spike phase $\psi^1=\mathrm{mod}(t,T_1)$ and $\psi^2=\mathrm{mod}(t,T_2)$, respectively, is also shown. Here t is the spike time. During 1:1 mode locking to T_1, $\sigma_{T1}<\sigma_{T2}$, whereas for 1:1 mode locking to T_2, $\sigma_{T2}<\sigma_{T1}$. (c) The winding number was determined on a grid of A_2 and I values (A_1 was 0.4). The areas with the same winding number were coded as follows, (black) mode locking to T_1, from top to bottom, 2:1, 3:2, 1:1, and 1:2; (cross hatched) mode locking to T_2, from top to bottom, 2:1 and 1:1; (striped) quasiperiodic mode locking, (top) $1/\tau=1/T_1+1/T_2$ and (bottom) $2/T_1-1/T_2$. (B),(C) In phase return maps, the phase ψ_{n+1} of the next spike time t_{n+1} was plotted vs the current phase ψ_n of t_n. The scale is the same for all graphs and is shown in Ca. The phase was calculated with respect to (B) T_1 and (C) T_2. The amplitude was $A_1=A_2=0.125$ and (a) $I=1.17$ ($p_1=q_1=1$); (b) $I=1.10$ (no rational winding number was found); (iii) $I=1.09$ ($p_2=q_2=1$). Other parameters: $T_1=2$, $T_2=2\sqrt{2}$. Averages were over (Aa), (Ab) 1600 spikes after discarding the first 400; and (Ac) 3200 spikes after discarding the first 800.

As A_2 was increased, mode locking to T_1 became unstable for large q_1, and in some current ranges p_2/q_2 mode locking was obtained instead. When both A_1 and A_2 were large, steps were obtained with an average interspike interval τ for which neither T_1/τ nor T_2/τ was rational. However, τ could be expressed as

$$\frac{1}{\tau}=\frac{p_1}{q_1}\frac{1}{T_1}+\frac{p_2}{q_2}\frac{1}{T_2}, \tag{6}$$

with integer values, possibly negative, for p_1, p_2, q_1, and q_2. In this case the neuron was mode locked to a linear combination with rational coefficients of both periods—quasiperiodic mode locking [36]. In Fig. 6(Ac) two examples are shown, $\tau=1.1715$, with $1/\tau=1/T_1+1/T_2$ and $\tau=1.5468$, with $1/\tau=2/T_1-1/T_2$. Note that in the latter case p_2 was negative.

The most prominent mode-locking regions were associated with $p_1=q_1=1$ (and $p_2=0$) and $p_2=q_2=1$ (and $p_1=0$). The spike trains for $p_1=q_1=1$ and $p_2=q_2=1$ and for an intermediate current value, were further analyzed using phase return maps [Figs. 6(B),6(C)]. During 1:1 mode locking to a periodic drive, the neuron spiked at a fixed phase and the interspike interval was constant and equal to the period of the drive. As a result the phase return map, the phase of the next spike time plotted vs the phase of current spike time, consisted of only one point, the fixed point of the map. Intrinsic noise introduced jitter in spike times, hence there was jitter in the spike phases. The deviations of the spike phase from the average spike phase were almost uncorrelated between consecutive cycles. The return map then consisted of a spherical cloud of points centered around the fixed point. During 1:1 mode-locking to the T_1 component in the quasiperiodic case there was jitter in the spike phase ψ^1, even without intrinsic noise. The jitter was due to the T_2-periodic drive component. The points in the phase return map were on a closed orbit, and the phases only took values between 0.58 and 0.78 [Fig. 6(Ba)]. However, the return map of ψ^2 formed an open orbit, and the phase had values between 0 and 1 [Fig. 6(Ca)]. The situation for 1:1 mode locking to the T_2 component was similar, the phase return map with respect to T_2 was a closed orbit [Fig. 6(Cc)], and now the ψ^1 return map was an open orbit [Fig. 6(Bc)]. We took a current value between the 1:1 T_1 and 1:1 T_2 mode-locking steps, that was not part of a step with a width of more than 10^{-5}. In that case, the orbits were discontinuous with part of the orbit missing [Figs. 6(Bb) and 6(Cb)]. The spike trains had a complicated structure; we could not establish whether they were aperiodic or chaotic or whether the winding number was irrational.

The stability of 1:1 T_1 mode locking against noise was investigated [Figs. 7(A),7(B)]. Three values for the driving current were used, $I=0.99$ on the left hand side of the step, $I=1.12$ in the middle of the step and 1.26 on the right hand side of the step. The phase return map consisted of closed orbits. The center of the orbits varied with the value of the current, from close to 1 on the left hand side to $\frac{1}{2}$ on the right hand side [Fig. 7(Ba)]. The interspike-interval return map also consisted of a closed orbit [Fig. 7(Aa)]. The orbits for different current values were arranged concentrically, the position of the center did not shift since the average ISI had to remain the same, however, the diameter of the orbit did vary.

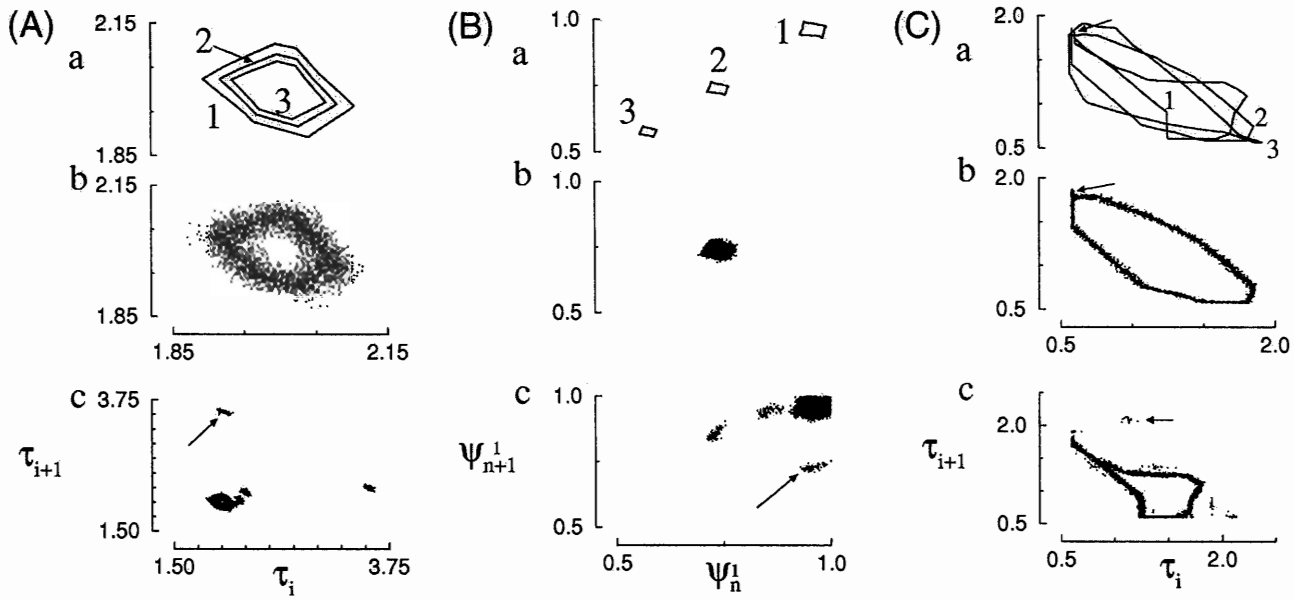

FIG. 7. (A), (C) interspike-interval and (B) spike-phase return maps for mode locking to a quasiperiodic current. (A),(B) 1:1 mode locking to T_1 for (a) three current values, (1) $I=0.99$, (2) $I=1.12$, and (3) $I=1.26$ without noise ($D=0$); (b) $I=1.12$ and $D=10^{-4}$ and (c) $I=0.99$, $D=10^{-4}$. The amplitudes were $A_1=0.4$ and $A_2=0.05$. The phase was calculated with respect to T_1. The scale in (Ac) is different from that in (Aa) and (Ab). The "donut" in the lower left hand side corner corresponds to the zero-noise orbit (1) in (Aa). (C) Quasiperiodic mode locking, the average interspike interval was $1/\tau=1/T_1+1/T_2$. Parameters were (a,1) $I=1.40$, (2) $I=1.46$, and (3) $I=1.515$ with $D=0$; (b) $I=1.46$, and $D=10^{-4}$; (c) $I=1.40$ and $D=10^{-4}$. The amplitudes were $A_1=0.4$ and $A_2=0.4$. Arrows in (Ac), (Bc), and (Cc) indicate the initial noise-induced deviation from the attractor; the arrows in (Ca) and (Cb) indicate a sharp excursion in the return map.

The attractor for the current value in the middle of the step was stable against noise. The return maps consisted of a cloud of points distributed around the zero-noise orbit. The attractor for $I=0.99$ was unstable against noise. Noise could prevent spikes from happening, leading to missing spikes and an interspike interval that was approximately two cycles. The resulting deviation in spike phase decayed back to zero over the course of a few cycles. The T_2 component acted as a deterministic noise source, the jitter based on $p_1:q_1$ mode locking $\sigma^{(p_1)}$ was approximately the sum of two terms,

$$(\sigma^{(p_1)})^2=\alpha_1 D+\alpha_2 A_2, \tag{7}$$

where α_1 and α_2 were proportionality constants. Hence, the T_2 component brought the neuron closer to a bifurcation point, and reduced the stability against noise.

Quasiperiodic mode locking was investigated using phase and interspike-interval return maps [Fig. 7(C)]. The $1/\tau=1/T_1+1/T_2$ mode-locking step was considered, three current values were used, $I=1.40$ on the left hand side of the step, $I=1.46$ in the middle of the step and 1.515 on the right hand side of the step. The phase return map of ψ^1 and ψ^2 consisted of an open orbit (not shown). The interspike interval return map was a closed orbit with a complex shape [Fig. 7(Ca)]. It had a remarkable feature as indicated by the arrows in Figs. 7(Ca) and 7(Cb). We made sure that the same feature was also obtained by direct integration of Eq. (1). In the presence of noise, the orbit in the middle of the step was stable [Fig. 7(Cb)], whereas the orbit near the edge of the step was unstable [Fig. 7(Cc)].

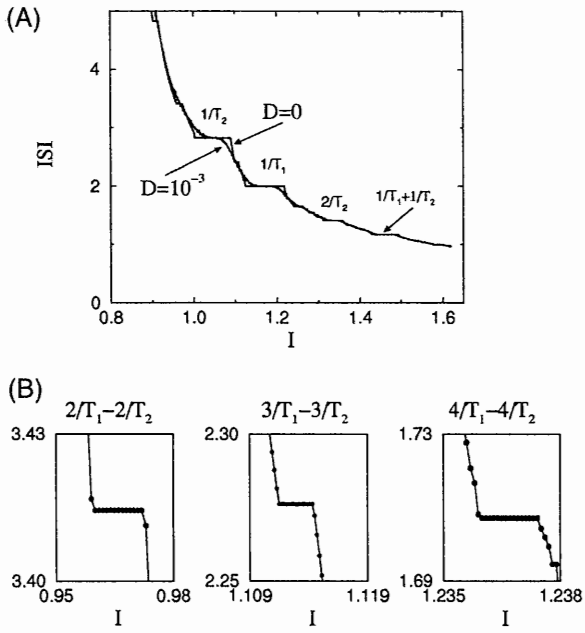

FIG. 8. Stability against noise of mode locking to a quasiperiodic piecewise constant current. (A) The average interspike interval (ISI) is plotted as a function of average driving current I for $D=0$ and $D=10^{-3}$. The most stable mode-locking ratios, expressed as $1/\tau=(p_1/q_1)1/T_1+(p_2/q_2)1/T_2$, are indicated in the graph. (B) Closeup of a few smaller mode-locking steps for $D=0$. The mode-locking ratios are given in the graph. Other parameters were, $T_1=2$, $T_2=2\sqrt{2}$, and $A_1=A_2=0.2$. Averages were over 3200 spikes after discarding a transient of 800.

For $A_1=A_2=0.4$ or 0.2, quasiperiodic mode-locking steps were also found for other ratios, including multiples of $1/T_1-1/T_2$: $1/\tau=n(1/T_1-1/T_2)$ for $n=2, 3, \ldots$ (Fig. 8). For these mode-locking steps we found only one attractor and the ISI return maps did not form closed orbits. Mode-locking steps for $1/\tau=\frac{1}{2}(2/T_1-1/T_2)$ and $\frac{1}{2}(1/T_1+1/T_2)$ were smaller than the current grid (2×10^{-4}) used in our simulations. However, when A_2 was much smaller than A_1, for instance, $A_1=0.4$ and $A_2=0.05$, these steps could be resolved. The dynamics had two attractors and the ISI return maps did *not* form closed orbits.

The noise stability of the mode-locking steps was investigated by comparing the ISI vs current curve for zero noise with that for $D=10^{-3}$ [Fig. 8(A)]. Only the 1:1 mode-locking steps to T_1, T_2 and the step with $1/\tau=1/T_1+1/T_2$ remained in the presence of noise. On these mode-locking steps there was only one attractor with an ISI return map that formed a closed orbit.

Thus, there were mode-locked solutions with a rational winding number with respect to either T_1 or T_2, or a rational combination thereof. In the former case, the non-mode-locked drive component generated deterministic jitter in the spike times. Steps with low values of p_1 and q_1 (p_2 and q_2) were more stable against intrinsic noise, and could also remain mode locked for a larger amplitude A_2 (A_1). In that case there were still q_1 (q_2) attractors. The stability of these attractors to intrinsic noise was reduced since the deterministic jitter would bring the attractor closer to a bifurcation point. For quasiperiodic mode locking there also could be multiple attractors. However, the corresponding steps were small. We did not establish a general relationship between the values of q_1 and q_2 and the number of attractors that would be observed. For most of the examples studied here, there was only one attractor for quasiperiodic mode locking. The steps with an ISI return map that formed a closed orbit were most stable. However, we did not establish whether this observation holds in general.

V. DISCUSSION

A. Noise stability of attractors and bifurcation structure

The bifurcation structure explained the differences in reliability between neurons driven by random and periodic fluctuating currents [26]. For the random fluctuating drive we found that there was one stable attractor [26]. We conjectured that in general neurons driven by a random fluctuating current have only one stable attractor [26]. Furthermore, we conjectured that for any given stimulus parameter the neuron was close to a bifurcation point for which only a few spike times changed discontinuously [26]. Only those spike times, and perhaps a few spike times immediately following a bifurcation spike time are unreliable. Hence, for a random drive, the overall reliability was reduced, but was still high for most parameter values.

When a periodic drive was injected into the model neuron, mode locking could occur [31,37–47]. During mode locking the neuron produced p spikes per q cycles and the spike train would repeat itself each q cycles (here p and q are positive integers). Hence, there could be multiple stable attractors with the same winding number. In model simulations we found that during $p:q$ mode locking there were q attractors. The attractor was most stable against noise during 1:1 mode locking, when there was only one attractor, and less reliable outside 1:1 mode locking. Hence, these theoretical results predict a reliability resonance for a periodic drive that is absent for a random drive. The reliability of pyramidal cells and interneurons in rat prefrontal cortical slices has been studied experimentally with sinusoidal current injection over a range of frequencies [23]. Pyramidal cells mode locked in the 5–20 Hz range, whereas interneurons mode-locked in the 5–50 Hz range [23]. Spike-time reliability was always highest during 1:1 mode locking [23,25].

A quasiperiodic drive is intermediate between a periodic and random fluctuating drive since it is not periodic but it does have deterministic structure. Here we report that the bifurcation structure of a neuron driven by a quasiperiodic drive [36] is similar to that for a periodically driven neuron. In particular, the mode-locking regions were organized in Arnold tongues. The widest steps corresponded to 1:1 mode locking to either one of the two components of the drive or quasiperiodic mode locking with small values for q_1 and q_2. On these steps there was only one attractor and the ISI return map formed a closed orbit. These steps were the most stable against noise and hence yielded the most reliable discharge. These results show that reliability is closely correlated to the number of attractors and the shape of return maps.

B. Reliability and Lyapunov exponents

The zero-noise stability of mode-locked solutions of periodically driven integrate-and-fire neurons was previously studied in terms of Lyapunov exponents [31,35],

$$\lambda=-1+\lim_{n\to\infty}\frac{1}{t_{n+1}-t_1}\sum_{k=0}^{n}\ln\left|\frac{I+f(t_{k+1})}{-1+I+f(t_{k+1})}\right|, \quad (8)$$

here t_k was the kth spike time on the attractor, I was the driving current, and $f(t)$ was the fluctuating driving current. All periodic mode-locked solutions had a negative Lyapunov exponent and were stable [31,35]. The periodic solutions with a low q value were more stable since the Lyapunov exponent was more negative (see Fig. 2 in Ref. [31]). When the neuron remained close to the attractor in the presence of intrinsic noise, the spike-time jitter was proportional to the noise standard deviation $\sqrt{D}$. The proportionality constant depended on the Lyapunov exponent: a more negative the Lyapunov coefficient resulted in a smaller proportionality constant, hence, less spike-time jitter. A detailed derivation is in preparation [32].

Stronger noise induced transitions between different attractors, or missing or extra spikes. The occurrence of these deviations from the attractor depended on the value of the Lyapunov exponent and the distance to a bifurcation point. As mentioned above, Lyapunov exponents characterized how fast a deviation from an attractor decayed to zero and determined the amplitude of noise-induced fluctuations around the zero-noise voltage trace. Deviations from attractors could occur when this amplitude was large enough to reach a bifur-

cation point. The Lyapunov exponent depended on the value of the driving current $f(t_k)$ at the spike times on the attractor [Eq. (8)]. Here, piecewise constant periodic currents were used and spikes occurred at a phase between $\frac{1}{2}$ and 1 (except for the parameters values used in Fig. 5). Hence, $f(t_k)$ always had the same value and the Lyapunov exponent only depended on the average interspike interval. As a result we could approximately delineate the effect of the bifurcation structure on the reliability of neural spike trains from that of the variation of $f(t)$. The result is that both the Lyapunov exponent and the distance to the bifurcation points are important determinants of the reliability: *the value of the Lyapunov exponent itself does not predict reliability in experiment, since transitions between attractors occur at physiological noise levels* [26].

C. Asymptotic attractor stability and reliability

In experiments reliability is assessed by presenting the same stimulus across multiple trials. In model simulations, this procedure corresponds to injecting the same input stimulus each time with an independent realization of the intrinsic noise (trial). The attractor reliability R_a is defined as the stability of the attractor against noise and is proportional to the inverse of the number of distinct spike trains obtained across a large number of trials [27]. Two spike trains are distinct when there is at least one spike time that is much further than $\sqrt{D}$ from any spike time in the other spike train (D is the variance of the intrinsic noise). When the neuron remains on one attractor, the *spike-time jitter* in the nth spike time ($n=1,2,\ldots$) across many trials is proportional to $\sqrt{D}$ and $R_a=1$ [32]. Noise can induce transitions between different attractors, or lead to missing or extra spikes. Distinct spike trains are then obtained across different trials, reliability is reduced and the spike-time jitter is not proportional to $\sqrt{D}$ anymore. In this paper, the asymptotic noise stability of attractors was determined based on one long trial with between 2000 and 10 000 spikes. When there are no transitions between attractors, missing or extra spikes, the *spike-phase jitter* is proportional to $\sqrt{D}$ and $R_a=1$. This procedure can underestimate the reliability compared with that obtained for multiple short trials since transitions between attractors during a long trial may not occur on short trials. However, this only affects the edges of mode-locking steps and the qualitative behavior of the reliability was the same (comparison not shown).

D. Future work

Neurons are more complex than the integrate-and-fire model neuron studied here. They contain many different membrane currents [48]. For instance, in model simulations using cells with a slow calcium-dependent potassium current (model as in Ref. [49]) convergence to the attractor could take up to one second. During that period the output spike train depended on the voltage and other internal variables such as calcium concentration at stimulus onset. Hence, during the transient the discharge might be unreliable. However, once the attractor was reached it was stable. How do these slow currents influence reliability under *in vivo* conditions? Neurons also display subthreshold membrane potential oscillations due to active currents [50–52]. The oscillation frequency depended on the type of neuron [23,53]. How does the bifurcation structure depend on these intrinsic oscillations? We plan to address these and other issues in future work.

ACKNOWLEDGMENTS

This work was funded by the Sloan-Swartz Center for Theoretical Neurobiology at the Salk Institute. I thank Jack Cowan, Jean-Marc Fellous, Jorge José, Terry Sejnowski, and Peter Thomas for discussions and useful suggestions. I thank Peter Thomas also for comments that have improved the presentation of the paper.

APPENDIX

For clarity, the notation in this appendix differs from that in the main text as follows. The constant depolarizing current I and fluctuating current $f(t)$ are combined into a fluctuating current denoted by $I(t)$. The two current values of the piecewise constant current will be denoted by subscripts 0 and 1, and the two components of the quasiperiodic current will be indicated by superscripts A and B. In the following four sections the analytical spike-time maps used in the numerical simulations are derived for the periodic piecewise constant drive without and with noise, and for the quasiperiodic piecewise constant drive without and with noise, respectively.

Neuron driven by a periodic piecewise constant current

The neuron is driven by a piecewise constant current $I(t)$ with period T, $I(t)=I_0$ when $\mathrm{mod}(t,T)<T_1$ and it is I_1 when $\mathrm{mod}(t,T)\geq T_1$. [Note that in the notation of the main text, $I_0=I-A$, $I_1=I+A$, and $T_1=T/2$.]

The solution to

$$\frac{dV}{dt}=-V+I(t),$$

with initial condition $V(t_1)=0$ is

$$V(t_2)=e^{-t_2}[h(t_2)-h(t_1)],$$

where

$$\begin{aligned} h(t)&=\int_0^t ds\, e^s I(s)\\ &=\sum_{n=1}^{N} e^{(n-1)T}\int_0^T ds\, e^s I(s)+e^{NT}\int_0^{\tau} ds\, e^s I(s)\\ &=\alpha\frac{1-e^{NT}}{1-e^{T}}+e^{NT}r(\tau), \end{aligned}$$

with $\tau=t-NT$,

$$r(\tau)=\int_0^{\tau} ds\, e^s I(s)=I_0(e^{\tau}-1), \quad \tau<T_1$$

$$=\alpha_1+I_1(e^{\tau}-e^{T_1}), \quad \tau\geq T_1$$

and

$$\alpha_1=I_0(e^{T_1}-1),$$

$$\alpha=\alpha_1+I_1(e^{T}-e^{T_1}).$$

A spike is generated when $V(t_2)=1$, yielding

$$h(t_2)-h(t_1)=e^{t_2};$$

using $t_1=N_1T+\tau_1$ and $t_2=N_2T+\tau_2$, we get

$$e^{N_2T+\tau_2}=\frac{\alpha}{1-e^T}(e^{N_1T}-e^{N_2T})+e^{N_2T}r(\tau_2)-e^{N_1T}r(\tau_1).$$

Combining all the terms containing τ_2 on the left hand side yields

$$e^{\tau_2}=\beta_{\pm}+e^{-\Delta NT}\gamma_{\pm},$$

with

$$\beta_+=\frac{1}{I_0-1}\left[\frac{\alpha}{1-e^T}+I_0\right],$$

$$\beta_-=\frac{1}{I_1-1}\left[\frac{\alpha}{1-e^T}-\alpha_1+I_1e^{T_1}\right]$$

and

$$\gamma_+=\frac{1}{I_0-1}\left[-\frac{\alpha}{1-e^T}+r(\tau_1)\right],$$

$$\gamma_-=\frac{1}{I_1-1}\left[-\frac{\alpha}{1-e^T}+r(\tau_1)\right],$$

where $\Delta N=N_2-N_1$. The solution to the γ_+ equation has to satisfy $0\leq\tau_2<T_1$ and the solution to the γ_- equation has to satisfy $T_1\leq\tau_2<T$. All different values $\Delta N=0,1,\ldots$ were tried until a solution was found.

Neuron with intrinsic noise driven by a periodic piecewise constant current

In the presence of intrinsic noise, the dynamics is

$$\frac{dV}{dt}=-V+I(t)+\xi(t),$$

with $\langle\xi(t)\rangle=0$, $\langle\xi(t)\xi(t')\rangle=D\delta(t-t')$. The equation for the next spike time t_2, starting from $V(t_1)=0$, is

$$V(t_2)=e^{-t_2}[h(t_2)-h(t_1)]+\lambda\chi=1,$$

where χ is Gaussian white noise with mean zero and unit variance, and

$$\lambda=\sqrt{\frac{D}{2}[1-e^{-2(t_2-t_1)}]}. \tag{A1}$$

Here, we assume that the noise trajectory $\xi(t)$ leading to χ at t_2 does not lead to a threshold crossing prior to t_2. Preliminary simulations using direct integration yield a spike-time variance similar to that obtained via the algorithm discussed here.

The resulting equation is squared to remove the square root,

$$[h(t_2)-h(t_1)-e^{t_2}]^2=\frac{D}{2}(e^{2t_2}-e^{2t_1})\chi^2,$$

yielding,

$$\left[\frac{\alpha}{1-e^T}(e^{-\Delta NT}-1)+r(\tau_2)-e^{-\Delta NT}r(\tau_1)-e^{\tau_2}\right]^2$$

$$=\frac{D\chi^2}{2}(e^{2\tau_2}-e^{2\tau_1-2\Delta NT}),$$

which is equivalent to

$$(\eta_{\pm}x+\delta_{\pm})^2=\frac{D\chi^2}{2}(x^2-e^{2\tau_1-2\Delta NT}),$$

where $x=e^{\tau_2}$, $\eta_+=I_0-1$, $\eta_-=I_1-1$, and

$$\delta_+=\frac{\alpha}{1-e^T}(e^{-\Delta NT}-1)-e^{-\Delta NT}r(\tau_1)-I_0,$$

$$\delta_-=\frac{\alpha}{1-e^T}(e^{-\Delta NT}-1)-e^{-\Delta NT}r(\tau_1)+\alpha_1-I_1e^{T_1}.$$

The result is a quadratic equation in x,

$$\left(\eta_{\pm}^2-\frac{D\chi^2}{2}\right)x^2+2\delta_{\pm}\eta_{\pm}x+\left(\delta_{\pm}^2+\frac{D\chi^2}{2}e^{2\tau_1-2\Delta NT}\right)\equiv ax^2+2bx+c=0, \tag{A2}$$

with a solution

$$x=-\frac{b}{a}\pm\frac{1}{a}\sqrt{b^2-ac}. \tag{A3}$$

The resulting algorithm is as follows. Generate a Gaussian deviate χ, and calculate $r(\tau_1)$ and $\eta_{\pm}$. Calculate $\delta_{\pm}$, a, b, and c for a given ΔN and solve the quadratic equation. Iterate over $\Delta N=0,1,\ldots$ until a solution is obtained for the correct sign of χ that satisfies $0\leq\tau_2<T_1$ for the δ_+ equation *or* $T_1\leq\tau_2<T$ for the δ_- equation.

Neuron driven by a quasiperiodic piecewise constant current

The neuron is driven by a sum of two periodic piecewise constant currents, $I(t)=I^A(t)+I^B(t)$, with $I^A=I_0^A$ when $0 \leqslant \mathrm{mod}(t,T^A)<T_1^A$ and $I^A=I_1^A$ when $T_1^A \leqslant \mathrm{mod}(t,T^A)<T^A$, likewise, $I^B=I_0^B$ when $0 \leqslant \mathrm{mod}(t,T^B)<T_1^B$ and $I^B=I_1^B$ when $T_1^B \leqslant \mathrm{mod}(t,T^B)<T^B$. (In the notation of the main text, $I_0^A=I/2-A_1$, $I_1^A=I/2+A_1$, $I_0^B=I/2-A_2$, $I_1^B=I/2+A_2$, $T_1^A=T_1/2$, and $T_1^B=T_2/2$.)

Starting from $V(t_1)=0$, the equation for the next spike time t_2 is again given by

$$V(t_2)=e^{-t_2}[h(t_2)-h(t_1)]=1. \tag{A4}$$

However, now $h(t)$ is the sum of two terms,

$$h(t)=\int_0^t ds\, e^s I(s)=h^A(t)+h^B(t),$$

with

$$h^A(t)=\alpha^A\frac{1-e^{N^AT^A}}{1-e^{T^A}}+e^{N^AT^A}r^A(\tau^A),$$

$$h^B(t)=\alpha^B\frac{1-e^{N^BT^B}}{1-e^{T^B}}+e^{N^BT^B}r^B(\tau^B),$$

and

$$r^A(\tau^A)=I_0^A(e^{\tau^A}-1), \quad \tau^A<T_1^A$$
$$=\alpha_1^A+I_1^A(e^{\tau^A}-e^{T_1^A}), \quad \tau^A\geqslant T_1^A,$$
$$r^B(\tau^B)=I_0^B(e^{\tau^B}-1), \quad \tau^B<T_1^B$$
$$=\alpha_1^B+I_1^B(e^{\tau^B}-e^{T_1^B}), \quad \tau^B\geqslant T_1^B,$$
$$\alpha^A=\alpha_1^A+I_1^A(e^{T^A}-e^{T_1^A}),$$
$$\alpha^B=\alpha_1^B+I_1^B(e^{T^B}-e^{T_1^B}),$$
$$\alpha_1^A=I_0^A(e^{T_1^A}-1),$$
$$\alpha_1^B=I_0^B(e^{T_1^B}-1),$$

where $t=N^AT^A+\tau^A=N^BT^B+\tau^B$. With the substitution $t_1=N_1^AT_1^A+\tau_1^A=N_1^BT_1^B+\tau_1^B$ and $t_2=N_2^AT_2^A+\tau_2^A=N_2^BT_2^B+\tau_2^B$, Eq. (A4) reads

$$e^{\tau_2^A+\Delta N^AT^A}=e^{-N_1^AT^A}[h^A(t_2)-h^A(t_1)+h^B(t_2)-h^B(t_1)]$$
$$=\frac{\alpha^A}{1-e^{T^A}}(1-e^{\Delta N^AT^A})+e^{\Delta N^AT^A}r^A(\tau_2^A)-r^A(\tau_1^A)$$
$$+\frac{\alpha^B}{1-e^{T^B}}(e^{\Delta_1}-e^{\Delta_2})+e^{\Delta_2}r^B(\tau_2^A-\Delta)$$
$$-e^{\Delta_1}r^B(\tau_1^B),$$

where $\Delta N^A=N_2^A-N_1^A$, $\Delta=N_2^BT^B-N_2^AT^A$, $\Delta_1=N_1^BT^B-N_1^AT^A$, $\Delta_2=N_2^BT^B-N_1^AT^A$ and $\tau_2^B=\tau_2^A-\Delta$. Combining the terms that contain $e^{\tau_2^A}$ yields

$$e^{\tau_2^A}(\eta_\pm^A+\eta_\pm^B)+\delta+\delta_\pm^A+\delta_\pm^B=0,$$

with

$$\eta_+^A=e^{\Delta N^AT^A}(I_0^A-1),$$
$$\eta_-^A=e^{\Delta N^AT^A}(I_1^A-1),$$
$$\eta_+^B=e^{\Delta_2-\Delta}I_0^B,$$
$$\eta_-^B=e^{\Delta_2-\Delta}I_1^B,$$

and

$$\delta_+^A=e^{\Delta N^AT^A}(-I_0^A),$$
$$\delta_-^A=e^{\Delta N^AT^A}(\alpha_1^A-I_1^Ae^{T_1^A}),$$
$$\delta_+^B=e^{\Delta_2}(-I_0^B),$$
$$\delta_-^B=e^{\Delta_2}(\alpha_1^B-I_1^Be^{T_1^B}),$$
$$\delta=\frac{\alpha^A}{1-e^{T^A}}(1-e^{\Delta N^AT^A})-r^A(\tau_1^A)+\frac{\alpha^B}{1-e^{T^B}}(e^{\Delta_1}-e^{\Delta_2})$$
$$-e^{\Delta_1}r^B(\tau_1^B).$$

For each value of N_2^A and N_2^B, there are four possible solutions for $e^{\tau_2^A}$. The sign of the A drive at time t_2 is denoted by S^A and the sign of the B drive is S^B. Each combination of $S^A=\pm$ and $S^B=\pm$ could be a solution. The real solution needs to satisfy, $0\leqslant\tau_2^A<T_1^A$ for $S^A=+$ *or* $T_1^A\leqslant\tau_2^A<T^A$ for $S^A=-$, and $0\leqslant\tau_2^B<T_1^B$ for $S^B=+$ *or* $T_1^B\leqslant\tau_2^B<T^B$ for $S^B=-$, where, as before, $\tau_2^B=\tau_2^A-\Delta$. The algorithm uses different values of N_2^A and N_2^B until a solution that satisfies the constraints is found. The tried values N_2^A and N_2^B are ordered such that consecutive values of $t=\max(N_2^AT^A,N_2^BT^B)$ increase monotonically.

Neuron with intrinsic noise driven by a quasiperiodic piecewise constant current

In the presence of noise Eq. (A4) reads

$$V(t_2)=e^{-t_2}[h(t_2)-h(t_1)]+\lambda\chi=1,$$

where λ is given by Eq. (A1). Using $t_1=N_1^AT_1^A+\tau_1^A$ and $t_2=N_2^AT_2^A+\tau_2^A$, we obtain

$$e^{-N_1^A T^A}[h(t_2)-h(t_1)]-e^{\tau_2^A+\Delta N^A T^A} + \sqrt{\frac{D}{2}(\exp[2\tau_2^A+2\Delta N^A T^A]-e^{2\tau_1^A})}\chi=0, \quad \text{(A5)}$$

this is rewritten as

$$xC_1+C_2+\sqrt{\frac{D}{2}(x^2e^{2\Delta N^A T^A}-e^{2\tau_1^A})}\chi=0, \quad \text{(A6)}$$

with $x=e^{\tau_2^A}$, $C_1=\eta_\pm^A+\eta_\pm^B$, and $C_2=\delta+\delta_\pm^A+\delta_\pm^B$ with the η's and δ's defined as in the preceding section. x is one of the two solutions of the quadratic equation,

$$(xC_1+C_2)^2=\frac{D\chi^2}{2}(x^2e^{2\Delta N^A T^A}-e^{2\tau_1^A}),$$

rewritten as

$$ax^2+2bx+c=0,$$

with solution

$$x=-\frac{b}{a}\pm\frac{1}{a}\sqrt{b^2-ac},$$

where,

$$a=C_1^2-\frac{D\chi^2}{2}e^{2\Delta N^A T^A},$$

$$b=C_1C_2,$$

$$c=C_2^2+\frac{D\chi^2}{2}e^{2\tau_1^A}.$$

Different values for N_2^A and N_2^B are tried as described in the preceding section.

[1] M. Shadlen and W. Newsome, J. Neurosci. **18**, 3870 (1998).
[2] M. Berry, D. Warland, and M. Meister, Proc. Natl. Acad. Sci. U.S.A. **94**, 5411 (1997).
[3] D. Warland, P. Reinagel, and M. Meister, J. Neurophysiol. **78**, 2336 (1997).
[4] D. Reich *et al.*, J. Neurophysiol. **77**, 2836 (1997).
[5] M. Berry and M. Meister, J. Neurosci. **18**, 2200 (1998).
[6] G. Buracas, A. Zador, M. DeWeese, and T. Albright, Neuron **20**, 959 (1998).
[7] W. Bair, Curr. Opin. Neurobiol. **9**, 447 (1999).
[8] P. Kara, P. Reinagel, and R. Reid, Neuron **27**, 635 (2000).
[9] P. Reinagel, D. Godwin, S. Sherman, and C. Koch, J. Neurophysiol. **81**, 2558 (1999).
[10] P. Reinagel and R. Reid, J. Neurosci. **20**, 5392 (2000).
[11] M. Shadlen and W. Newsome, Curr. Opin. Neurobiol. **4**, 569 (1994).
[12] W. Softky, Curr. Opin. Neurobiol. **5**, 239 (1995).
[13] A. Gur, M. Beylin, and D. Snodderly, J. Neurosci. **17**, 2914 (1997).
[14] M. Oram, M. Wiener, R. Lestienne, and B. Richmond, J. Neurophysiol. **81**, 3021 (1999).
[15] M. Wiener and B. Richmond, J. Neurophysiol. **81**, 2861 (1999).
[16] Z. Mainen and T. Sejnowski, Science **268**, 1503 (1995).
[17] L. Nowak, M. Sanchez-Vives, and D. McCormick, Cereb. Cortex **7**, 487 (1997).
[18] A. Tang, A. Bartels, and T. Sejnowski, Cereb. Cortex **7**, 502 (1997).
[19] A. Warzecha, J. Kretzberg, and M. Egelhaaf, Curr. Biol. **8**, 359 (1998).
[20] G. Cecchi *et al.*, Proc. Natl. Acad. Sci. U.S.A. **97**, 5557 (2000).
[21] A. Warzccha, J. Kretzberg, and M. Egelhaaf, J. Neurosci. **20**, 8886 (2000).
[22] J. Kretzberg, M. Egelhaaf, and A. Warzecha, J. Comput. Neurosci. **10**, 79 (2001).
[23] J.-M. Fellous *et al.*, J. Neurophysiol. **85**, 1782 (2001).
[24] J. Hunter, J. Milton, P. Thomas, and J. Cowan, J. Neurophysiol. **80**, 1427 (1998).
[25] U. Beierholm *et al.*, J. Neurophysiol. **86**, 1858 (2001).
[26] P. Tiesinga, P. Thomas, J.-M. Fellous, and T. Sejnowski, Soc. Neurosci. Abstracts **27**, 821.12 (2001).
[27] P. Tiesinga, J.-M. Fellous, and T. Sejnowski, Neutral Computation (to be published).
[28] C. Koch, *Biophysics of Computation* (Oxford University Press, New York, 1999).
[29] W. Press, S. Teukolsky, W. Vetterling, and B. Flannery, *Numerical Recipes* (Cambridge University Press, Cambridge, 1992).
[30] D. Hansel *et al.*, Neural Comput. **10**, 467 (1998).
[31] S. Coombes and P. C. Bressloff, Phys. Rev. E **60**, 2086 (1999).
[32] P. Thomas and P. Tiesinga (unpublished).
[33] T. Tateno, J. Stat. Phys. **92**, 675 (1999).
[34] T. Tateno and Y. Jimbo, Phys. Lett. A **271**, 227 (2000).
[35] S. Coombes, Phys. Lett. A **255**, 49 (1999).
[36] J. Cartwright, D. Gonzalez, and O. Piro, Phys. Rev. E **59**, 2902 (1999).
[37] B. Knight, J. Gen. Physiol. **59**, 767 (1972).
[38] B. Knight, J. Gen. Physiol. **59**, 734 (1972).
[39] J. Keener, F. Hoppensteadt, and J. Rinzel, SIAM (Soc. Ind. Appl. Math.) J. Appl. Math. **41**, 503 (1981).
[40] H. Read and R. Siegel, Neuroscience **75**, 301 (1996).
[41] A. Longtin and D. R. Chialvo, Phys. Rev. Lett. **81**, 4012 (1998).
[42] T. Shimokawa, A. Rogel, K. Pakdaman, and S. Sato, Phys. Rev. E **59**, 3461 (1999).
[43] S. Tanabe, S. Sato, and K. Pakdaman, Phys. Rev. E **60**, 7235 (1999).
[44] T. Shimokawa, K. Pakdaman, and S. Sato, Phys. Rev. E **60**, R33 (1999).
[45] K. Pakdaman, Phys. Rev. E **63**, 041907 (2001).
[46] P. Tiesinga and T. Sejnowski, Network **12**, 215 (2001).

[47] P. Tiesinga, J.-M. Fellous, J. José, and T. Sejnowski, Network **13**, 41 (2002).
[48] G. Shepherd, *Synaptic Organization of the Brain*, 4th ed. (Oxford University Press, Oxford, 1998).
[49] P. Tiesinga, J.-M. Fellous, J. José, and T. Sejnowski, Hippocampus **11**, 251 (2001).
[50] R. Llinas, A. Grace, and Y. Yarom, Proc. Natl. Acad. Sci. U.S.A. **88**, 897 (1991).
[51] I. Lampl and Y. Yarom, Neuroscience **87**, 325 (1997).
[52] L. Leung and C. Yin, Brain Res. **553**, 261 (1991).
[53] F. Pike *et al.*, J. Physiol. (London) **529**, 205 (2000).